

State selective differential cross sections for single and double
electron capture in $He^{1,2+} - He$ and $p - He$ collisions

by

M. S. Schöffler¹, J. Titze¹, L. Ph. H. Schmidt¹, T. Jahnke¹, O. Jagutzki¹, H. Schmidt-Böcking¹, R. Dörner¹ and I. Mančev²

¹ *Institut für Kernphysik, Universität Frankfurt, 60486 Frankfurt, Germany*

² *Department of Physics, Faculty of Sciences and Mathematics,
University of Niš, P.O. Box 224, 18000 Niš, Serbia*

PACS: 34.70.+e - Charge transfer.

Abstract. Using the COLTRIM technique, scattering angle differential cross sections for single and double electron capture in collisions of protons and $He^{1,2+}$ projectiles with helium atoms for incident energies of 60–630 keV/u are measured. We also report new theoretical results obtained by means of four-body one-channel distorted wave models (CDW-BFS, CDW-BIS and BDW), and find mixed agreement with the measured data.

I. Introduction

Electron transfer is a very fundamental process in physics and chemistry. In nuclear physics the strong forces allows protons or neutrons being captured in nuclear collisions, in astrophysics the gravitational force can lead to capture of stellar objects and in chemistry capture is often a part of a chemical reaction. Ion-atom-collisions provide an ideal testground where the quantum mechanical electron capture processes can be explored over a wide parameter space of trajectories (impact parameters) and velocities.

The key variable controlling the mechanism responsible for electron transfer is the projectile velocity. At small velocities electron transfer happens via the formation of intermediate molecular states. At intermediate velocities capture is governed by the overlap of the wave functions of initial and final state in momentum space, displaced by the projectile velocity. At even higher velocities electron capture is more likely dominated by the Thomas-process, an inter atomic double scattering, which accelerates the target electron to projectile velocity and leads to a distinct structure [21, 22, 26, 25, 27, 28] in the scattering angle dependence. Finally at the highest velocities, radiative capture dominates [24].

Using the COLTRIMS-technique [30, 31, 32] the projectile scattering angle dependence of the electron transfer probabilities for different final states (ground state and/or target/projectile excitations) we measured. Especially at higher velocities only a few experiments exist in which the different final states were separated. In the most experiments the data have been integrated over all final states. But for example only 30 % of the total cross section for single electron capture (SC) He^{2+}/He at 60 keV/u lead to the ground state. Or in the most common system, proton-Helium, (up to 630 keV/u) about 20 % are found in an excited state. For a quantitative comparison with theory as well as for an interpretation of the scattering angle differential data it is, however, essential to separate the final state. Summation of the scattering angle dependence over excited states of projectile and or target can wash-out much of the structure in the individual channels [19] and obscures the comparison with theory. In this paper we concentrate on the capture to the electronic ground state without excitation of the remaining target electron.

II. Experiment

Capture processes (single and multiple) typically lead to small projectile

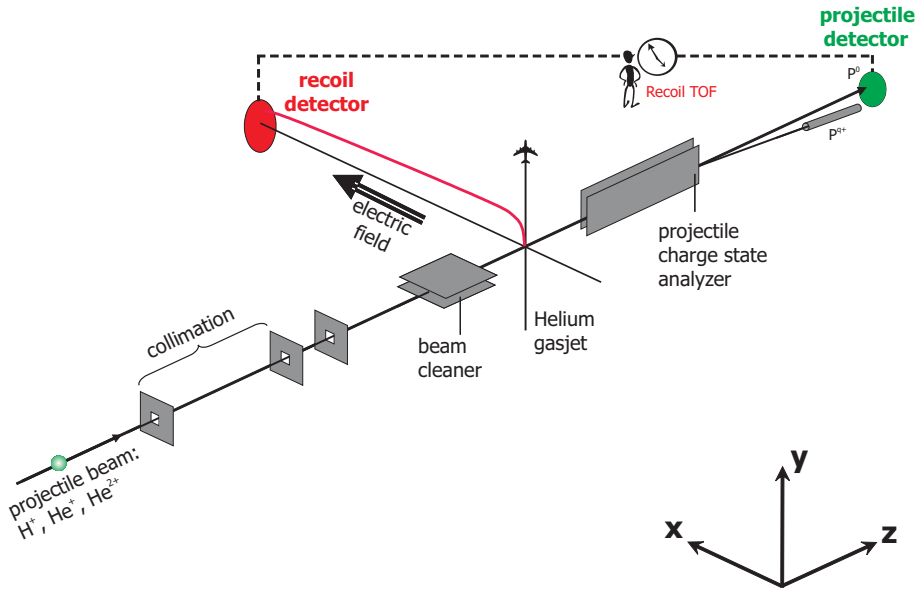


Figure 1: Draft of the experimental setup.

scattering angles θ , corresponding to a few atomic units (a. u.) of transverse momentum exchange between target and projectile. Since no electron is emitted to the continuum, from momentum conservation the transverse momentum transfer to the projectile is equal and opposite to the transverse momentum of the recoiling ion [29]. In the present experiment we measure both in coincidence, the projectile scattering and the transverse component of the recoil ion momentum.

The experimental data have been measured at the Van de Graaff accelerator at the Institut für Kernphysik at the University of Frankfurt. The final state is given by a He⁺ recoiling ion and the down charged ejectile. Between both collision partners momentum and energy conservation has to be fulfilled. Thus measuring one would be enough to get the full kinematical information. We used the COLTRIMS technique (COLd Target Recoil Ion Momentum Spectroscopy) to measure both particles in coincidence (see figure 1 and [30, 31, 32] for some general reviews).

The target is provided by a super sonic gas jet. Through a 30 μm nozzle helium gas is expanded into a high vacuum chamber at a driving pressure of 30 bar. 5 mm above the nozzle a skimmer (\varnothing 0.3 mm) cuts out the central part of the gas jet. Before entering the target chamber, the gas jet is collimated by a second aperture (0.5 mm in diameter). Due to the adiabatic expansion and the collimation the gas atoms have a momentum uncertainty of about 0.1 a. u. in all three dimensions. A target jet diameter of 1 mm and a density of 5×10^{11} atoms/cm² was reached at the intersection region with the projectile beam. Finally the gas jet is pumped differentially to achieve a low Helium background

pressure in the target chamber (1×10^{-8} mbar). The projectile beam (H^+ , He^+ and He^{2+}), coming from the Van de Graaff accelerator was collimated by two sets of adjustable slits to a beam-spot size of $0.5 \times 0.5 \text{ mm}^2$ at the target. To provide the He^{2+} beam a gas stripper was used. 15 cm upstream the target, the beam was cleaned from charge state impurities with a set of electrostatic deflectors. Behind the target a second set of electrostatic deflectors was used to separate the primary beam from the ejectiles that changed their charge during the collision. The latter were detected by a 40 mm position- and time-sensitive multi channel plate (MCP) detector with delay line readout [33]. The $\text{He}^{1+,2+}$ recoil ions were accelerated by a weak electrostatic field of 4.8 V/cm (at the target) and projected onto a 80 mm position- and time-sensitive MCP detector with delay line anode for position read out. To maximize the resolution by minimizing the perturbing influence of the extended reaction volume a three dimensional time- and space focussing field geometry was used (see figure 2 in [23]). Including drift tube, the overall distance from target to detector is 1.4 m.

By measuring the time of flight (19 μs for He^+ and 13.4 μs for He^{2+}) we obtained the charge state and the momentum in field direction. From the position of impact we calculated the momenta in the direction perpendicular to the electric field.

Along the beam axis (z) the momentum of the recoil ion is directly related to the Q-value of the reaction [19]:

$$p_z = -\frac{Q}{v_P} - \frac{v_P}{2} \quad (1)$$

Each final electronic state corresponds to a well defined discrete longitudinal ion momentum. In reality these peaks are broadened by the target temperature and the resolution of the spectrometer. Their width is the total momentum resolution, which was found to be 0.1 a. u. (limited by the target temperature). The measured experimental values for all final states have been normalized to total cross sections, taken from [34]. The projectile scattering angles was also measured in coincidence. It was used, however, only to roughly clean the data from background (by checking for momentum conservation in the plane perpendicular to the initial beam axis). Instead the projectile scattering angle θ was deduced from the momenta transferred to the target, for which we achieve a much better resolution than for the projectile momentum itself. The spectrometer's geometry and voltages were chosen to yield 4π acceptance angle for ions up to 10 a. u. transverse momentum.

III. Theory

A. Single electron capture

Let us first consider single charge exchange in collisions of completely stripped projectiles with a helium-like target: $Z_P + (Z_T; e_1, e_2)_i \rightarrow (Z_P; e_1)_{f_1} + (Z_T; e_2)_{f_2}$, where $Z_P(Z_T)$ is the charge of the projectile (target). The parentheses symbolize the bound state whose quantum numbers are given by collective labels i, f_1

and f_2 . We shall denote by $\vec{s}_{1,2}$ and $\vec{x}_{1,2}$ the position vectors of the electrons $e_{1,2}$ relative to Z_P and Z_T , respectively. The inter-electron distance r_{12} is given by $r_{12} = |\vec{s}_1 - \vec{s}_2| = |\vec{x}_1 - \vec{x}_2|$. Let further \vec{R} be the vector of the internuclear axis directed from Z_T to Z_P . In the entrance channel, it is convenient to introduce \vec{r}_i as a relative vector of Z_P with respect to the center of mass of $(Z_T; e_1, e_2)_i$. Further in the exit channel, let \vec{r}_f be the relative vector of the center of mass of $(Z_P; e_1)_{f_1}$ with respect to the center of mass of $(Z_T; e_2)_{f_2}$.

The asymptotic channel states $\Phi_{i,f}^\pm$ which satisfy correct boundary conditions read as follows:

$$\Phi_i^+ = \varphi_i(\vec{x}_1, \vec{x}_2) \exp[i\vec{k}_i \cdot \vec{r}_i + i\nu_i \ln(k_i r_i - \vec{k}_i \cdot \vec{r}_i)], \quad (2)$$

$$\Phi_f^- = \varphi_P(\vec{s}_1) \varphi_T(\vec{x}_2) \exp[-i\vec{k}_f \cdot \vec{r}_f - i\nu_f \ln(k_f r_f - \vec{k}_f \cdot \vec{r}_f)], \quad (3)$$

where $\nu_i = Z_P(Z_T - 2)/v$, $\nu_f = (Z_T - 1)(Z_P - 1)/v$ with v being the incident velocity, and k_i, k_f are the initial and final wave vectors. The initial bound state is denoted by $\varphi_i(\vec{x}_1, \vec{x}_2)$, whereas bound state wave functions of the atomic system $(Z_P; e_1)$ and $(Z_T; e_2)$ are labeled by $\varphi_P(\vec{s}_1)$ and $\varphi_T(\vec{x}_2)$, respectively.

The transition amplitudes in the continuum distorted wave - Born initial state (CDW-BIS) approximation [4, 3] and the continuum distorted wave - Born final state (CDW-BFS) [1, 2] are given as:

$$T_{if}^{CDW-BIS} = \langle \chi_f^- | U_f^\dagger | \Phi_i^+ \rangle, \quad T_{if}^{CDW-BFS} = \langle \Phi_f^- | U_i | \chi_i^+ \rangle. \quad (4)$$

Here, the perturbation potentials U_i and U_f and corresponding distorted waves χ_i^\pm are chosen as in the CDW-4B method [5, 6]:

$$U_i = V(R, s_2) - \vec{\nabla}_{x_1} \ln \varphi_i(\vec{x}_1, \vec{x}_2) \cdot \vec{\nabla}_{s_1}, \quad (5)$$

$$U_f = V(R, s_2) - V(r_{12}, x_1) - \vec{\nabla}_{s_1} \ln \varphi_f(\vec{s}_1) \cdot \vec{\nabla}_{x_1}, \quad (6)$$

with

$$V(R, s_2) = Z_P(1/R - 1/s_2), \quad V(r_{12}, x_1) = (1/x_1 - 1/r_{12}), \quad (7)$$

$$\begin{aligned} \chi_i^+ &= N^+(\nu_P) \mathcal{N}^+(\nu) e^{i\vec{k}_i \cdot \vec{r}_i} \varphi_i(\vec{x}_1, \vec{x}_2) {}_1F_1(i\nu_P, 1, i\nu s_1 + i\vec{v} \cdot \vec{s}_1) \\ &\quad \times {}_1F_1(-i\nu, 1, i\vec{k}_i r_i - i\vec{k}_i \cdot \vec{r}_i), \end{aligned} \quad (8)$$

$$\begin{aligned} \chi_f^- &= \mathcal{N}^-(\nu) N^-(\nu_T) \varphi_P(\vec{s}_1) \varphi_T(\vec{x}_2) e^{-i\vec{k}_f \cdot \vec{r}_f} {}_1F_1(-i\nu_T, 1, -i\nu x_1 - i\vec{v} \cdot \vec{x}_1) \\ &\quad \times {}_1F_1(i\nu, 1, -i\vec{k}_f r_f + i\vec{k}_f \cdot \vec{r}_f), \end{aligned} \quad (9)$$

where $\nu_T = (Z_T - 1)/v$, $\nu_P = Z_P/v$, $\nu = Z_P(Z_T - 1)/v$, $N^-(\nu_T) = \Gamma(1 + i\nu_T) e^{\pi\nu_T/2}$, $N^+(\nu_P) = \Gamma(1 - i\nu_P) e^{\pi\nu_P/2}$, $\mathcal{N}^\pm(\nu) = \Gamma(1 \pm i\nu) e^{-\pi\nu/2}$. The symbol

${}_1F_1(a, b, c)$ denotes the confluent hypergeometric function. The eikonal approximation $\vec{R} \simeq -\vec{r}_f$, $\vec{R} \simeq \vec{r}_i$ is also used. It is readily verified that the distorted waves $\chi_{i,f}^\pm$ satisfy the proper boundary conditions $\chi_{i,f}^\pm \rightarrow \Phi_{i,f}^\pm$ when $r_{i,f} \rightarrow \infty$.

The explicit expressions for matrix elements can be written as:

$$T_{if}^{CDW-BFS} = N^+(\nu_P) \int \int \int d\vec{x}_1 d\vec{x}_2 d\vec{R} e^{i\vec{k}_i \cdot \vec{r}_i + i\vec{k}_f \cdot \vec{r}_f} \varphi_P^*(\vec{s}_1) \varphi_T^*(\vec{x}_2) \mathcal{L}(R) [V(R, s_2) \times \varphi_i(\vec{x}_1, \vec{x}_2) {}_1F_1(i\nu_P, 1, i\nu s_1 + i\vec{v} \cdot \vec{s}_1) - \vec{\nabla}_{x_1} \varphi_i(\vec{x}_1, \vec{x}_2) \cdot \vec{\nabla}_{s_1} {}_1F_1(i\nu_P, 1, i\nu s_1 + i\vec{v} \cdot \vec{s}_1)],$$

$$T_{if}^{CDW-BIS} = [N^-(\nu_T)]^* \int \int \int d\vec{x}_1 d\vec{x}_2 d\vec{R} e^{i\vec{k}_i \cdot \vec{r}_i + i\vec{k}_f \cdot \vec{r}_f} \varphi_i(\vec{x}_1, \vec{x}_2) \mathcal{R}(R) \left\{ {}_1F_1(i\nu_T, 1, i\nu x_1 + i\vec{v} \cdot \vec{x}_1) [V(R, s_2) - V(r_{12}, x_1)] \varphi_P^*(\vec{s}_1) \varphi_T^*(\vec{x}_2) - \varphi_T^*(\vec{x}_2) \vec{\nabla}_{s_1} \varphi_P^*(\vec{s}_1) \cdot \vec{\nabla}_{x_1} {}_1F_1(i\nu_T, 1, i\nu x_1 + i\vec{v} \cdot \vec{x}_1) \right\},$$

with

$$\mathcal{L}(R) = (vR + \vec{v} \cdot \vec{R})^{i\nu_f} (vR - \vec{v} \cdot \vec{R})^{i\nu} = \rho^{2iZ_P(Z_T-1)/v} (vR + \vec{v} \cdot \vec{R})^{-i(Z_T-1)/v}, \quad (10)$$

$$\mathcal{R}(R) = (vR - \vec{v} \cdot \vec{R})^{i\nu_i} (vR + \vec{v} \cdot \vec{R})^{i\nu} = (\rho)^{2i\nu_i} (vR + \vec{v} \cdot \vec{R})^{iZ_P/v}, \quad (11)$$

where unimportant phase factors are dropped. Here $\vec{\rho}$ is a component of the vector of the internuclear distance perpendicular to the Z -axis.

The analytical calculation outlined in the ref. [1] provides the matrix elements of the CDW-BFS model in terms of two dimensional real quadrature, whereas in the case of CDW-BIS approximation the T -matrix elements can be analytically reduced [3, 4] to five-dimensional integral which must be evaluated numerically. Reason for this is that the term $1/r_{12}$ in the perturbation U_f requires an additional three-dimensional integral. All numerical integrations are carried out by means of the Gauss-Legendre quadrature after scaling of variables. In both models, the standard Cauchy regularization of the whole integrand is accomplished before applying the numerical integrations.

During the construction of the hybrid-type models, such as CDW-BIS and CDW-BFS, the main idea has been to approximate the exact wave function *in one* of the channels, by using a simple analytical function which can well describe the principal interaction region, and, to preserve correct boundary conditions in both channels. Hence, according to these models the captured electron is treated in an asymmetrical manner in the entrance and exit channel.

In this work, the explicit calculation of the matrix elements for single electron capture are carried out by using the two-parameter wave function of Silverman *et al* [7] for the initial state of helium target: $\varphi_i(\vec{x}_1, \vec{x}_2) = N[e^{-\alpha_1 x_1 - \alpha_2 x_2} + e^{-\alpha_2 x_1 - \alpha_1 x_2}]/\pi$, where $N = [1/\alpha_1^3 + 1/\alpha_2^3 + 16/(\alpha_1 + \alpha_2)^3]^{-1/2}$. Despite its very simple form in this function [7] the radial static correlations are taken into account to within nearly 90%.

B. Double electron capture

Next, we consider typical double charge exchange in collisions of completely stripped projectiles with heliumlike target: $Z_P + (Z_T; e_1, e_2)_i \longrightarrow (Z_P; e_1, e_2)_f + Z_T$. In the present paper the second order four-body theory called Born distorted wave (BDW) approximation [8, 9] is employed. According to this model the transition amplitude (for example prior form) is given by:

$$T_{if}^{BDW} = \langle \Phi_f^- | U_i | \chi_i^+ \rangle, \quad (12)$$

where the asymptotic channel state Φ_f^- reads as follows:

$$\Phi_f^- = \varphi_f(\vec{s}_1, \vec{s}_2) \exp[-i\vec{k}_f \cdot \vec{r}_f - i\nu_f \ln(k_f r_f - \vec{k}_f \cdot \vec{r}_f)], \quad (13)$$

with $\nu_f = Z_T(Z_P - 2)/v$. Now the \vec{r}_f denotes relative vector of Z_P with respect to the center of mass of $(Z_T; e_1, e_2)_f$ in the exit channel. The initial distorted wave χ_i^+ is given in the eikonal limit:

$$\begin{aligned} \chi_i^+ = & [N^+(\nu_P)]^2 \mathcal{N}^+(\nu_{PT}) e^{i\vec{k}_i \cdot \vec{r}_i} \varphi_i(\vec{x}_1, \vec{x}_2) {}_1F_1(i\nu_P, 1, i\nu s_1 + i\vec{v} \cdot \vec{s}_1) \\ & {}_1F_1(i\nu_P, 1, i\nu s_2 + i\vec{v} \cdot \vec{s}_2) {}_1F_1(-i\nu_{PT}, 1, ik_i r_i - i\vec{k}_i \cdot \vec{r}_i), \end{aligned} \quad (14)$$

provided that U_i is chosen as

$$U_i = \sum_{i=1}^2 \vec{\nabla}_{x_i} \ln \varphi_i(\vec{x}_1, \vec{x}_2) \cdot \vec{\nabla}_{s_i}. \quad (15)$$

Here, the symbols ν_{PT} and ν_P are defined as: $\nu_{PT} = Z_P Z_T / v$, $\nu_P = Z_P / v$. Hence, the BDW is hybrid-type model which in the entrance and exit channel coincides, respectively, with the CDW-4B [10] and CB1-4B [11] method. The BDW approximation introduces a normalized scattering state for every value of r_f in the final channel, in which the reduction of the BDW to the CB1-4B model takes place.

The differential cross sections are defined by the following relation

$$\frac{d\sigma d\Omega}{=} \frac{\mu_i \mu_f}{4\pi^2} |T_{if}|^2 [a_0^2 / sr] \quad (16)$$

where $\mu_i = M_P(M_T + 2)/(M_P + M_T + 2)$, $\mu_f = M_T(M_P + 2)/(M_P + M_T + 2)$ with $M_{P,T}$ being mass of the projectile/target nucleus. The scattering angle θ is identified from the relation $\eta = 2\mu_{PT}v \sin(\theta/2)$, where μ_{PT} is the reduced mass of the projectile and target nucleus.

IV. Results and discussion

p+He collisions

Theoretical results for differential cross sections for single electron capture in $p-He$ collisions at impact energies 60, 100, 150, 300 keV obtained by means

of four body CDW-BFS model are compared with the measured data in Figure 2a-d. The displayed theoretical results in Fig. 2 are obtained by means of a two parameter Silverman *et al.* [7] orbitals for the initial helium bound state. The computations are performed also with the help of simplest one parameter orbitals of Hylleraas [12] as well as four-parameter wave functions of Löwdin [13]. It is observed that the differential cross section for the here considered problem is not strongly sensitive to the choice of the bound state wave functions, since the difference between corresponding results is less than 20%. In general the main peak in the differential cross sections between 0 and 0.5 mrad is mediated by the momentum transfer of the captured electron and reflects an image of the initial electron momentum distribution. Scattering angles below 0.55 mrad are known to be dominated by momentum transfer mediated by the electron (see [35, 36, 37] and [27] for capture reactions) while all larger deflection angles the scattering is dominated by momentum exchange between the nuclei.

The theory yields good agreement as well as in shape as in absolute height with the experimental data at small scattering angles for all energies, also for other measurements [14, 15]. However, for larger scattering angles theory predicts a slightly different angular and v_P -dependency. Particularly the CDW-BFS-approximation predicts a strong Thomas-peak contribution ($\theta_{lab} = (1/M_P) \sin 60^\circ \simeq 0.472 \text{ mrad}$) with increasing v_P , which is clearly not present in the data. At impact energies of 300 keV/u theory increasingly underestimates the large scattering angles clearly..

${}^3\text{He}^{2+} + {}^4\text{He}$ collisions (Single capture)

Theoretical results for single electron capture in ${}^3\text{He}^{2+} + \text{He}$ collisions at impact energies 60, 150, 300, 450 and 630 keV/u for angular region from 0 to 1.5 mrad obtained by means of four body CDW-BIS model are compared with the measured data in Figures 3. The Thomas peak for this reaction is at $\theta_{lab} \simeq 0.154 \text{ mrad}$. The CDW-BIS model exhibits an unphysical and experimentally unobserved dip before and after the Thomas peak region, due to mutual cancelation among the various terms in the potential U_f given by eq.(6). Despite the proper inclusion of the Rutherford scattering, the CDW-BIS approximation predicts the differential cross sections which are in disagreement with measurements in the region where the internuclear scattering takes over. Nevertheless, the experimental resolution is clearly good enough to make such structures visible, if they would exist. So thus at 60 keV/u the theoretical curve is considerably higher than the corresponding experimental data at larger scattering angle.

${}^3\text{He}^+ + {}^4\text{He}$ collisions (Single capture)

This is a true five-body problem of the type $(Z_P; e_3) + (Z_T; e_1, e_2)_i \rightarrow (Z_P; e_1, e_3)_{f_1} + (Z_T; e_2)_{f_2}$. Instead of this, in the present work we theoretically consider the following model reaction: $Z_P^{eff} + (Z_T; e_1, e_2)_i \rightarrow (Z_P^{eff}; e_1)_{f_1} + (Z_T; e_2)_{f_2}$. In this model the presence of the projectile electron is taken into account only through a screening effect. The two-electron atom in the exit channel is described by a hydrogenic model. Within this approximation, the

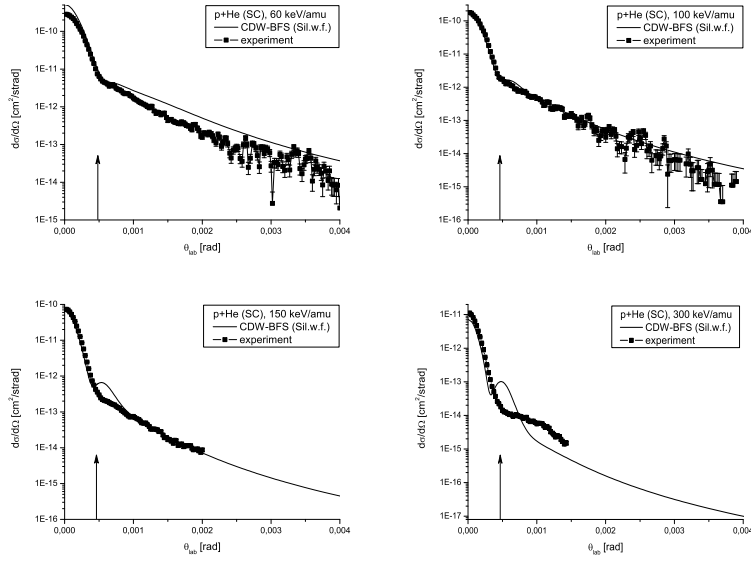


Figure 2: The differential cross sections $dQ_{if}/d\Omega$ ($cm^2/strad$) as a function of scattering angle θ (rad) for single electron capture to the groundstate in $p - He$ collisions at 60, 100, 150 and 300 keV/u . Both cross sections and the scattering angle are in the laboratory system. The symbol \blacksquare relates to the present measurements, the full line represents the results obtained by means of the CDW-BFS model (present computation). The arrow indicated the location of the electron-nuclear Thomas-peak.

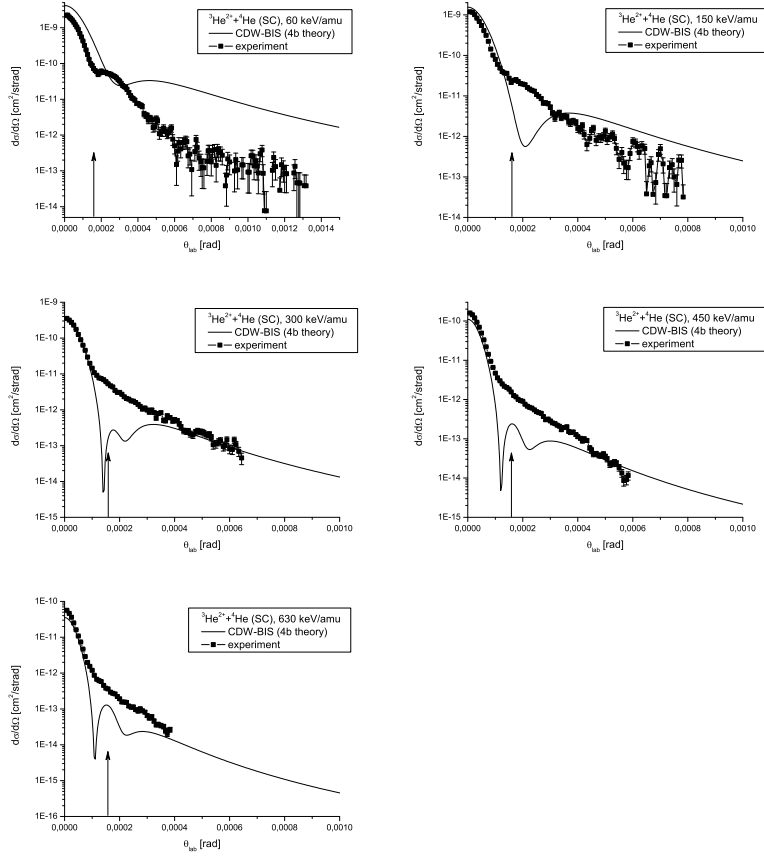


Figure 3: The differential cross sections $dQ_{if}/d\Omega(\text{cm}^2/\text{strad})$ as a function of scattering angle $\theta(\text{rad})$ for single electron capture to the groundstate in $\text{He}^{2+} - \text{He}$ collisions at 60, 150, 300, 450 and 630 keV/u. Both cross sections and the scattering angle are in the laboratory system. The symbol \blacksquare relates to the present measurements, the solid line represents the results obtained by means of the CDW-BIS model (present computation). The arrow indicated the location of the electron-nuclear Thomas-peak.

binding energy is $E_f = -[Z_P^{eff}]^2/2$, where the effective charge is $Z_P^{eff} = Z_P - 5/16$. Such a choice of the Z_P^{eff} provides a satisfactory description for a K -shell electron near the Bohr radius. The corresponding hydrogenic $1s$ wave function is very close to the actual K -shell orbital (for example Hartree-Fock $1s$ wave function). However, this fixed effective charge does not produce the correct experimental binding energy. It also cannot reflect the true dynamic situation of the captured electron in the newly formed helium atom. Of course, other choices for the effective charge are possible (see e.g. [17]). The results of the computation, using CDW-BIS theory, of such a model reaction are represented in Fig. 4a-d.

It can be seen from figure 4, that this satisfactory theoretical approach cannot reproduce the data. At larger scattering angle we find a similar disagreement as for the collision systems discussed previously. But now also in the small angle regime ("the electronic peak") the v_P dependence is not well predicted. Similar to the impact of He^{2+} the theory shows an unphysical dip around the Thomas peak.

${}^3He^{2+} + {}^4He$ collisions (Double capture)

Theoretical results for differential cross sections in ${}^3He^{2+} + He$ collisions at incident energies 60, 150, 200 and 300 keV/u are displayed in Fig. 5a-d. As can be seen, the BDW-calculations are in general in the electron-peak regime a factor 2 below the experimental data, but agree well in shape. At larger scattering angles (nuclear scattering), experimental and theoretical slope differ slightly. The displayed theoretical and experimental results present only the transition $1s^2 \rightarrow 1s^2$. The present computations for double capture are performed by using one-parameter orbitals of the Hylleraas type [12] in both the entrance and exit channel. For example, the initial state bound state of the helium target is described by $\varphi_i(\vec{x}_1, \vec{x}_2) = (\gamma^3/\pi)exp[-\gamma(x_1 + x_2)]$, where $\gamma = 1.6875$ is the effective charge.

The computations of differential cross sections are carried out also by means of the four-body boundary-corrected continuum intermediate state (BCIS) approximation which has been introduced by Belkić [18]. The essential difference between the BCIS and BDW is in the perturbation potentials. Namely, in the BDW model one encounters the typical gradient operator potentials which are familiar from the CDW-4B approximation [10]. The role of these perturbations in the BCIS method is played by the conventional first Born-type multiplicative operators, which are the same as in the CB1-4B approach [11]. It is observed that the behavior of the angular distribution obtained in the BCIS model is altogether quite similar to that in the BDW approximation for the considered impact energies.

Occupied states

As explained from the experimental values we can deduce the fraction of different occupied final states (transfer to groundstate, target-, projectile- and target&projectile excitation). For the impact He^{2+} it couldn't be distinguished

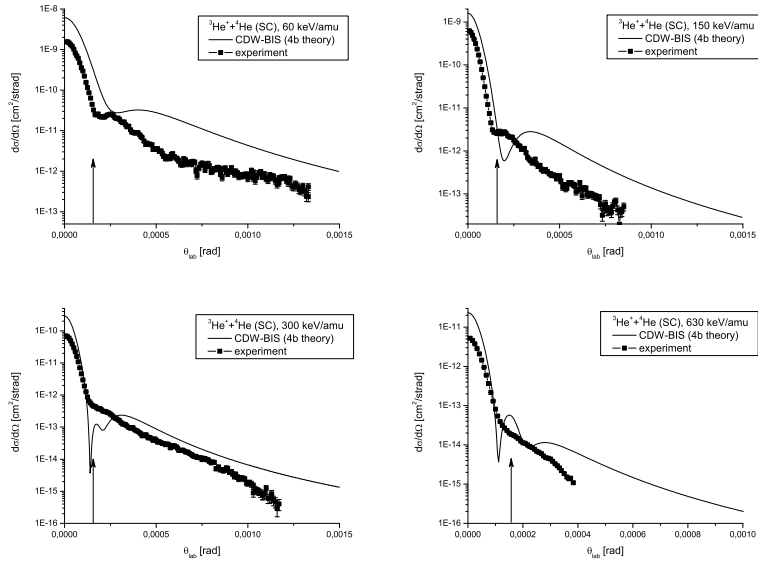


Figure 4: The differential cross sections $dQ_{if}/d\Omega$ ($cm^2/strad$) as a function of scattering angle θ (rad) for single electron capture to the groundstate in $He^+ - He$ collisions at 60, 150, 300 and 630 keV/u . Both cross sections and the scattering angle are in the laboratory system. The symbol \blacksquare relates to the present measurements, the solid line represents the results obtained by means of the CDW-BIS model (present computation). The arrow indicated the location of the electron-nuclear Thomas-peak.

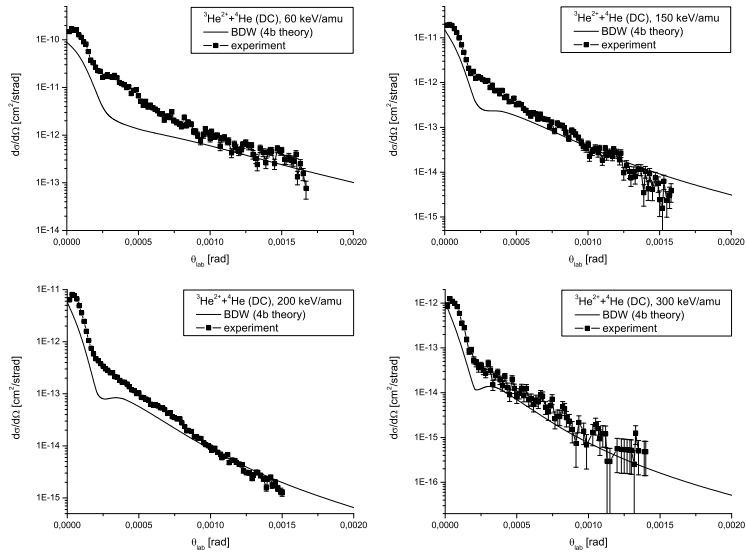


Figure 5: The differential cross sections $dQ_{if}/d\Omega$ ($cm^2/strad$) as a function of scattering angle θ (rad) for double electron capture to the groundstate in $He^+ - He$ collisions at 60, 150, 200 and 300 keV/u . Both cross sections and the scattering angle are in the laboratory system. The symbol \blacksquare relates to the present measurements, the full line represents the results obtained by means of the BDWS approximation (present computation).

whether the target (He^+) or the projectile (either He^+) is excited. Hence the sum of both is presented in table 1 below.

| collision system | $\sigma(P_{1s}, T_{1s})$ | $\sigma(P_{nl}, T_{nl})$ | $\sigma(P_{nl}, T_{1s})$ | $\sigma(P_{nl}, T_{nl})$ |
|------------------------|--------------------------|--------------------------|--------------------------|--------------------------|
| H^+ 60 keV/u SC | 6.5×10^{-17} | 2.3×10^{-18} | 1.5×10^{-17} | 1.2×10^{-18} |
| H^+ 100 keV/u SC | 2.5×10^{-17} | 1.0×10^{-18} | 6.8×10^{-18} | 6.5×10^{-19} |
| H^+ 150 keV/u SC | 7.3×10^{-18} | 3.0×10^{-19} | 2.0×10^{-18} | 1.4×10^{-19} |
| H^+ 300 keV/u SC | 7.0×10^{-19} | 4.6×10^{-20} | 1.6×10^{-19} | 1.0×10^{-20} |
| He^{2+} 40 keV/u SC | 7.9×10^{-17} | | 2.2×10^{-16} | 3.0×10^{-18} |
| He^{2+} 60 keV/u SC | 5.7×10^{-17} | | 1.5×10^{-16} | 4.4×10^{-18} |
| He^{2+} 150 keV/u SC | 1.8×10^{-17} | | 2.2×10^{-17} | 2.7×10^{-18} |
| He^{2+} 300 keV/u SC | 3.9×10^{-17} | | 3.4×10^{-18} | 4.3×10^{-19} |
| He^{2+} 450 keV/u SC | 1.4×10^{-17} | | 9.0×10^{-19} | 7.4×10^{-20} |
| He^{2+} 630 keV/u SC | 3.4×10^{-17} | | 1.9×10^{-19} | 2.3×10^{-20} |
| He^+ 60 keV/u SC | 4.2×10^{-17} | 1.9×10^{-17} | 9.1×10^{-18} | 8.5×10^{-19} |
| He^+ 150 keV/u SC | 5.9×10^{-18} | 3.1×10^{-18} | 6.4×10^{-19} | 3.7×10^{-19} |
| He^+ 300 keV/u SC | 7.9×10^{-19} | 2.9×10^{-19} | 7.9×10^{-20} | 3.2×10^{-20} |
| He^+ 630 keV/u SC | 3.5×10^{-20} | 1.1×10^{-20} | 3.2×10^{-21} | 1.1×10^{-21} |
| He^{2+} 40 keV/u DC | 4.5×10^{-17} | - | 1.6×10^{-17} | - |
| He^{2+} 60 keV/u DC | 2.7×10^{-17} | - | 7.5×10^{-18} | - |
| He^{2+} 150 keV/u DC | 1.7×10^{-18} | - | 3.5×10^{-19} | - |
| He^{2+} 200 keV/u DC | 5.3×10^{-19} | - | 1.1×10^{-19} | - |
| He^{2+} 300 keV/u DC | 7.3×10^{-20} | - | 1.2×10^{-20} | - |

Table 1: Total cross sections for single and double electron transfer to the ground state $\sigma(P_{1s}, T_{1s})$, with target excitation $\sigma(P_{nl}, T_{nl})$, with projectile excitation $\sigma(P_{nl}, T_{1s})$ and target+projectile excitation $\sigma(P_{nl}, T_{nl})$, $n, l \geq 2$. The integral data have been normalized to [34].

V. Conclusions

In conclusion we have presented a systematic comparison of experimental data and theory for fully differential data of the most simple capture reactions in an intermediate range of projectile energies. At very small angles (the dominant contribution to the total capture cross section) the electron-transfer is mediated by the electron dynamics in the initial state, yielding an universal shape for all systems investigated. Theory and experiment agree quite well in shape and absolute height (beside double capture). At large scattering angles (nuclear scattering), we observe larger disagreement between theory and present measurement. These findings are in line with similar conclusion drawn in the last few years for ionization collisions [38, 41, 40]. Also for ionization surprising discrepancies between experiment and the most elaborated theoretical approaches persist. They are attributed currently to problems in describing correctly the nuclear and electron momentum exchange [39]. The delicate inter-

play of momentum exchange between nuclei and electrons in few body collision still poses a major challenge to theory today.

Acknowledgements

This work was supported by DFG, the BMBF, GSI, and Roentdek GmbH. I.M. acknowledges the support from Ministry of Science of the Republic of Serbia through Project No. 141029A.

References

- [1] I. Mančev, J. Phys. B: At. Mol. Opt. Phys., **36**, 93 (2003)
- [2] I. Mančev, V. Mergel and L. Schmidt, J. Phys. B: At. Mol. Opt. Phys., **36**, 2733 (2003)
- [3] I. Mančev, J. Comput. Meth. Sci. Eng. (JCMSE) **5**, 73 (2005)
- [4] I. Mančev, Europhys. Lett. **69**, 200 (2005)
- [5] Dž. Belkić, R. Gayet, J. Hanssen, I. Mančev and A. Nuñez, Phys. Rev. A, **56**, 3675 (1997)
- [6] I. Mančev, Phys. Rev. A, **60**, 351 (1999)
- [7] J.N.Silverman, O.Platas and F.A.Matsen, J.Chem.Phys. **32**, 1402 (1960)
- [8] Dž. Belkić, I. Mančev and M. Mudrinić, Phys. Rev. A **49**, 3646 (1994)
- [9] Dž. Belkić, Nucl. Inst. Meth. Phys. Res. B **86**, 62 (1994)
- [10] Dž. Belkić, I. Mančev, Phys. Scr. **45**, 35 (1992); *ibid* Phys. Scr. **46**, 18 (1993)
- [11] Dž. Belkić, J. Phys. B **26**, 497 (1993); Dž. Belkić, Phys. Rev. A **47**, 189 (1993)
- [12] E.Hylleraas, Z.Phys. **54**, 347 (1929)
- [13] P.Löwdin, Phys.Rev. **90**, 120 (1953)
- [14] S.W. Bross, S.M. Bonham, A.D. Gaus, J.L. Peacher, T. Vajnai, M. Schulz and H. Schmidt-Böcking, Phys. Rev. A **50**, 337 (1994)
- [15] P.J. Martin, K.Arnett, D.M. Blankenship, T.J. Kvale, J.L. Peacher, E.Redd, V.C. Sutcliffe, J.T. Park, C.D. Lin and J.H. McGuire, Phys. Rev. A **23**, 2858 (1981)
- [16] C.F. Barnett, H.T. Hunter, M.I. Kirkpatrick, I. Alvarez, C. Cisneros and R.A. Phaneuf, Oak Ridge National Laboratory Report No. ORNL-6068, Vol 1, (1990)
- [17] J.H. McGuire, N. Stolterfoht and P.R. Simony, Phys. Rev. A **24**, 97 (1981)

- [18] Dž. Belkić, Phys. Rev. A **47**, 3824 (1993)
- [19] V. Mergel, R. Dörner, J. Ullrich, O. Jagutzki, S. Lencinas, S. Nüttgens, L. Spielberger, M. Unverzagt, C. L. Cocke, R. E. Olson, M. Schulz, U. Buck, E. Zanger, W. Theisinger, M. Isser, S. Geis and H. Schmidt-Böcking, Phys. Rev. Lett., **74**, 2200, (1995)
- [20] R. Dörner, V. Mergel, L. Spielberger, O. Jagutzki, J. Ullrich and H. Schmidt-Böcking, Phys. Rev. A, **57**, 312, (1998)
- [21] L. H. Thomas, Proc. Roy. Soc. A, **114**, 561, (1927)
- [22] D. Fischer, K. Stochkel, H. Cederquist, H. Zettergren, P. Reinhed, R. Schuch, A. Källberg, A. Simonsson and H. T. Schmidt, Phys. Rev. A, **73**, 052713, (2006)
- [23] R. Dörner, V. Mergel, L. Spielberger, M. Achler, Kh. Khayyat, T. Vogt, H. Bräuning, O. Jagutzki, T. Weber, J. Ullrich, R. Moshhammer, M. Unverzagt, W. Schmitt, H. Khemliche, M.H. Prior, C. L. Cocke, J. Feagin, R.E. Olson and H. Schmidt-Böcking, Nucl. Instr. Meth. B, **124**, 225, (1997)
- [24] Th. Stöhlker, H. Geissel, H. Irnich, C. Kozhuharov, P. H. Mokler, G. Münzenberg, F. Nickel, C. Scheidenberger, T. Suzuki, M. Kucharski, A. Warczak, P. Rymuza, Z. Stachura, A. Kriessbach, D. Dauvergne, B. Dunford, J. Eichler, A. Ichihara and T. Shirai, Phys. Rev. Lett., **73**, 352, (1994)
- [25] E. Horsdal-Pedersen, C. L. Cocke and M. Stöckli, Phys. Rev. Lett., **50**, 1910, (1983)
- [26] H. Vogt, R. Schuch, E. Justiniano, M. Schulz and W. Schwab, Phys. Rev. Lett., **57**, 2256, (1986)
- [27] V. Mergel, R. Dörner, M. Achler, K. Khayyat, S. Lencinas, J. Euler, O. Jagutzki, S. Nüttgens, M. Unverzagt, L. Spielberger, W. Wu, R. Ali, J. Ullrich, H. Cederquist, A. Salin, C. J. Wood, R. E. Olson, Dž. Belkić, C. L. Cocke and H. Schmidt-Böcking, Phys. Rev. Lett., **79**, 387, (1997)
- [28] V. Mergel, R. Dörner, K. Khayyat, M. Achler, T. Weber, H. Schmidt-Böcking and H. J. Lüdde, Phys. Rev. Lett., **86**, 2257, (2001)
- [29] J. Ullrich, R. Olson, R. Dörner, V. Dangendorf, S. Kelbch, H. Berg, H. Schmidt-Böcking, J. Phys. B **22**, 627, (1989)
- [30] J. Ullrich, R. Moshhammer, R. Dörner, O. Jagutzki, V. Mergel, H. Schmidt-Böcking and L. Spielberger, J. Phys. B: At. Mol. Opt. Phys., **30**, 2917, (1997)
- [31] R. Dörner, V. Mergel, O. Jagutzki, L. Spielberger, J. Ullrich, R. Moshhammer and H. Schmidt-Böcking, Physics Reports, **330**, 95, (2000)

- [32] J. Ullrich, R. Moshhammer, A. Dorn, R. Dörner, L. Ph. H.Schmidt and H. Schmidt-Böcking, Rep. Prog. Phys., **66**, 1463, (2003)
- [33] O. Jagutzki, J. S. Lapington, L. B. C. Worth, U. Spillman, V. Mergel and H. Schmidt-Böcking, Nucl. Instr. and Meth. in Phys. Res. A, **477**, 256, (2002)
- [34] C. F. Barnett: *Atomic Data for Fusion, Collisions of H, H₂, He and Li Atoms with Atoms and Molecules*, edited by I. Alvarez, C. Cisneros and R. A. Phaneuf, Controlled Fusion Atomic Data Center, Springfield, Volume I, (1990)
- [35] E. Y. Kamber, C. L. Cocke, S. Cheng and S. L. Varghese, Phys. Rev. Lett. **60**, 2026, (1988)
- [36] R. Dörner, J. Ullrich, R. E. Olson and H. Schmidt-Böcking, Phys. Rev. Lett. **63**, 147, (1989)
- [37] A. Gensmantel, J. Ullrich, R. Dörner, R. E. Olson, K. Ullmann, E. Forberich, S. Lencinas, and H. Schmidt-Böcking, Phys. Rev. A **45**, 4572, (1992)
- [38] M. Schulz, R. Moshhammer, D. Fischer, H. Kollmus, D. H. Madison, S. Jones, and J. Ullrich, Nature (London) **422**, 48, (2003)
- [39] M. Schulz, M. Dürr, B. Najjari, R. Moshhammer and J. Ullrich, Phys. Rev. A **76**, 032712, (2007)
- [40] M. Foster, J. L. Peacher, M. Schulz, D. H. Madison, Zhangjin Chen and H. R. J. Walters, Phys. Rev. Lett. **97**, 093202, (2006)
- [41] J. Fiol, S. Otranto, and R. E. Olson, J. Phys. B: At. Mol. Opt. Phys., **39**, L285-L290, (2006).